## Title

Effects of Salinity-Induced Chemical Reactions on Biotite Wettability Changes under Geologic CO2 Sequestration Conditions



## Journal

Environmental Science & Technology Letters, 3(3)

## ISSN

2328-8930

## Authors

Zhang, Lijie
Kim, Yongman
Jung, Haesung
et al.

## Publication Date

2016-03-08

## DOI

10.1021/acs.estlett.5b00359

Peer reviewed

# Effects of Salinity-Induced Chemical Reactions on Biotite Wettability Changes under Geologic $CO_2$ Sequestration Conditions

Lijie Zhang[†], Yongman Kim[‡], Haesung Jung[†], Jiamin Wan[‡], and Young-Shin Jun[*,†]

[†] Department of Energy, Environmental and Chemical Engineering, Washington University, St. Louis, Missouri 63130, United States

[‡] Energy Geosciences Division, Lawrence Berkeley National Laboratory, Berkeley, California 94720, United States

*Environ. Sci. Technol. Lett.*, **2016**, *3* (3), pp 92–97

**DOI:** 10.1021/acs.estlett.5b00359

## Abstract

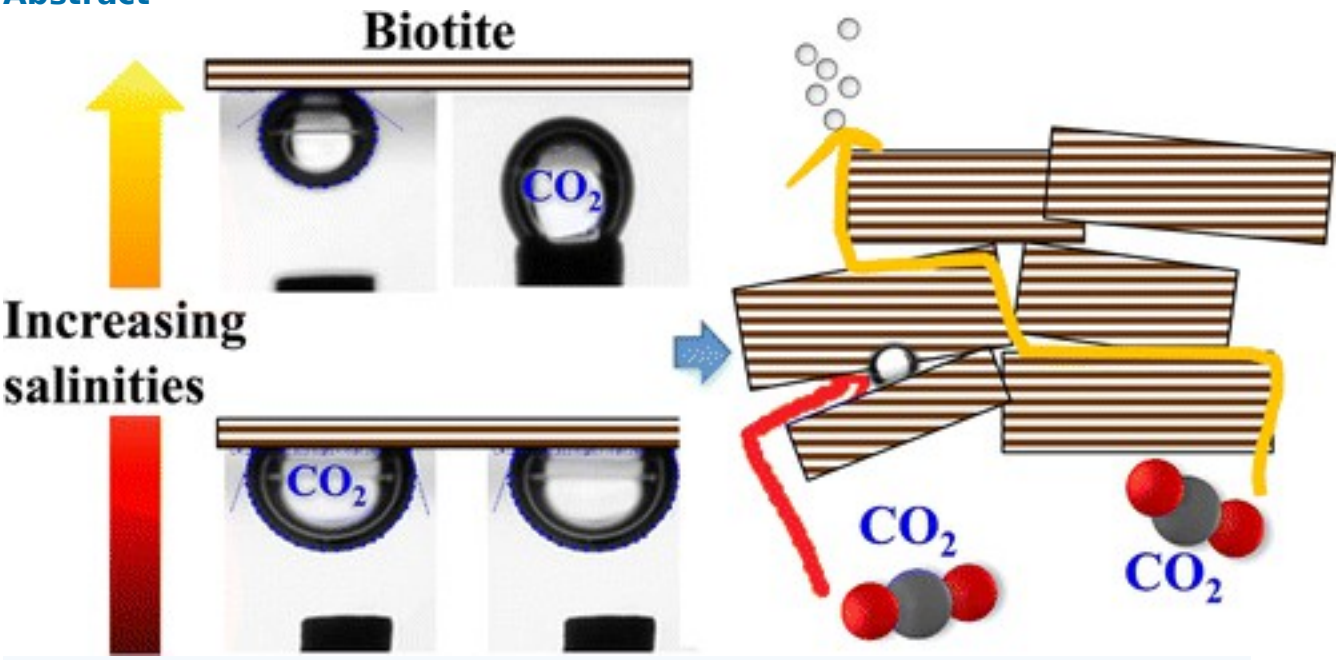


The wettability of rocks and minerals significantly affects the safety and efficiency of energy-related subsurface operations. Salinity is an important controlling factor in terms of wettability but has received limited attention. We studied the effects of salinity-induced chemical reactions on biotite's wettability changes under relevant subsurface conditions. Biotite was reacted at 95 °C and 102 atm of $CO_2$ for 70 h in solutions with salinities of 0, 0.1, 0.5, and 1.0 M NaCl. Then, static and dynamic water contact angles on reacted biotite basal surfaces were measured using a captive drop method. As a result of enhanced biotite dissolution at higher salinities, increased roughness, more negatively charged surfaces, and higher densities of hydroxyl groups on the biotite surfaces made biotite basal surface more hydrophilic. These results provide new information about the interplay of chemical

reactions and wettability alterations of minerals, providing a better understanding of $CO_2$ transport in subsurface environments.

## Introduction

In geologic $CO_2$ sequestration (GCS), the wettability of the reservoir rocks and minerals affects the mobility, residual trapping capacity, and caprock breakthrough pressures of the injected supercritical $CO_2$ ($scCO_2$).(1, 2) Previous experimental and modeling studies have shown that $scCO_2$, temperatures, pressures, and aqueous chemistries, such as salinity, all impact the wettability of the rocks and minerals.(3-7) For example, Chiquet et al. reported a transition from water-wet toward intermediate wettability for mica and quartz with increasing $CO_2$ pressures, and mica showed a more pronounced wettability alteration.(3)

Although the wettability of rocks and minerals has been widely investigated, the results show considerable uncertainties.(1, 8-11) In $CO_2$/water/silica systems, Jung et al. reported an increase in contact angles (CAs) with increasing salinity in the range of 0–5 M, whereas Wang et al. found a slight decrease in the range of 0–1.2 M.(8, 9) Both constant and increasing CAs with higher $CO_2$pressures were reported for silica.(8, 10) These uncertainties can result from varying surface roughnesses, surface contaminations, or surface chemical reactions during measurements.(12, 13) Mineral dissolution and secondary phase precipitation were observed even within a short time at field sites and in laboratory studies under GCS conditions.(14-19) In addition to direct effects of salinity on wettability caused by interfacial tension,(20) salinity-induced chemical reactions can change mineral surface properties, thus affecting wettability. However, no studies have systematically examined the effects of chemical reactions on mineral wettability alterations under GCS relevant conditions.

Deep saline aquifers are estimated to have a large capacity for $CO_2$ storage.(21-24) They contain highly saline brine, with the $Cl^-$ concentration generally falling in the range of 0.01–2.2 M.(25-27)For example, the Frio-I GCS site has a Na–Ca–Cl type brine with a salinity of ∼1.6 M.(27) At the Weyburn $CO_2$-enhanced oil recovery site, the $Cl^-$ concentration ranges from 0.4 to 1.0 M.(25) In addition, salinity compresses the electrical double layer, impacting wettability.(20) Salinity also affects mineral dissolution and secondary mineral formation.(28, 29) Hence, effects of salinity on mineral wettability alteration have been studied; however, the effects of salinity-induced chemical reactions on wettability changes have not been investigated.(3, 8, 9, 30)

Therefore, this study, conducted under conditions relevant to energy-related subsurface operations, seeks to systematically relate salinity-induced chemical reactions of biotite, a model mineral in caprocks (section S1 of the Supporting Information), with subsequent wettability changes, and to elucidate the mechanisms of wettability changes. Our findings will fill the urgent need to understand the unexplored relationships among salinity, chemical reactions, and wettability changes of minerals and thus will provide benefits for environmentally sustainable $CO_2$storage.

## Experimental Section

### Minerals and Chemicals

Biotite (Ward's Natural Science) was cleaved along the {001} basal plane to 80 ± 10 μm thick flakes that were cut into 2.5 cm × 2.5 cm squares. The biotite flakes were sonicated with acetone, ethanol, and 2-propanol to remove organic matter, then rinsed with deionized (DI) water, and dried with high-purity nitrogen gas. Clean biotite specimens were also ground using stainless steel blades and sieved to yield particles with sizes of 53–106 μm for further powder dissolution experiments. A more detailed explanation is available in section S1 of the Supporting Information.

### Methods

Biotite flake and powder dissolution experiments were conducted in a 300 mL high-temperature and high-pressure reactor (Parr Instrument Co.), as used in our previous studies (Figure S1 of the Supporting Information).(14, 15, 31, 32) To simulate subsurface environmental conditions, the temperature was 95 °C and the pressure was 102 atm of $CO_2$.(32, 33) The calculated initial pH was 3.16 (section S2 of the Supporting Information). Batch experiments were stopped after reaction for 70 h. The aqueous solutions from flake dissolution were filtered through a 0.2 μm polypropylene membrane and acidified in 1% trace metal nitric acid ($HNO_3$). The dissolved ion concentrations were then analyzed by inductively coupled plasma-optical emission spectrometry (ICP-OES, PerkinElmer Optima 7300 DV). The reacted biotite flakes were carefully rinsed with DI water, dried with high-purity nitrogen, and then immediately stored in tubes to avoid any contamination. All samples were treated the same way. Biotite basal surface morphology and roughness were then examined via atomic force microscopy (AFM) (Nanoscope V Multimode, Veeco).

Contact angles on prereacted biotite basal surfaces were measured using a captive drop method in a high-pressure and -temperature CA measurement chamber (Figure S2, Temco, IFT-10), as done in previous work by Jung and Wan.(8) During the measurement, the temperature and pressure of the chamber were kept at 48 ± 1 °C and 102 atm of $CO_2$, respectively. The temperature was

considerably lower than the reaction temperature (95 °C) to retard any biotite dissolution during CA measurements (Figure S3 of the Supporting Information). Both static and dynamic CAs were measured by generating a $CO_2$ bubble on a biotite basal surface. ImageJ, combined with DropSnake and Low-Bond Axisymmetric Drop Shape Analysis (LB-ADSA) plugins, was used to analyze the CAs. As a convention, the CA values reported hereafter refer to the water phase. The smallest and largest CAs during dynamic CA measurements were reported as the receding ($\theta_R$) and advancing ($\theta_A$) CAs, respectively. The length of the contact line was measured from the $CO_2$ receding images.

Reacted biotite powders were measured for ζ potential by electrophoretic mobility analyzer (Malvern, Zetasizer). Surface functional groups of oxygen of the reacted dry powders were analyzed by X-ray photoelectron spectroscopy (XPS).

Detailed information about the methods can be found in sections S3–S5 of the Supporting Information.

## Results and Discussion

### Higher Salinity Enhances Biotite Dissolution

Biotite dissolution was significantly enhanced with increasing salinities. Figure 1 shows the released concentrations of interlayer K and the framework cations Si, Al, Fe, and Mg after biotite flake (Figure 1A) and powder (Figure 1B) dissolution in DI water (i.e., 0 M NaCl) and 0.1, 0.5, and 1.0 M NaCl solutions with 102 atm of $CO_2$ at 95 °C for 70 h. Ion-exchange reactions between interlayer K in biotite and $Na^+$ in the solution were promoted at higher salinities, leading to higher concentrations of K released into the solutions. Higher salinity also enhanced the release of framework cations.

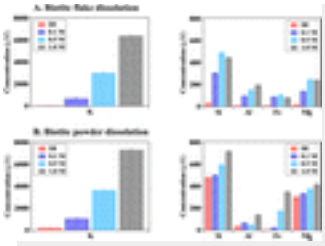

Figure 1. Aqueous concentrations of K, Si, Al, Fe, and Mg from the dissolution of biotite flakes (A) and biotite powders (B) after 70 h in solutions with different salinities (0, 0.1, 0.5, and 1.0 M NaCl) at 102 atm of $CO_2$ and 95 °C.

The surface morphology was altered by salinity as observed in AFM analyses of biotite basal surfaces (Figure 2). After reaction in DI water for 70 h, the basal surface of biotite was still smooth and almost unaltered (Figure 2A). With higher salinities, deeper and more abundant cracks formed

on the biotite basal surfaces, with crack depths of 4.2 ± 1.3, 7.8 ± 2.4, and 56.0 ± 8.4 nm for 0.1, 0.5, and 1.0 M NaCl samples, respectively. This trend was consistent with more significant ion-exchange reactions of aqueous $Na^+$ and interlayer K in biotite at higher salinities, which was reported to contribute to crack formation.(14) Formation of cracks on biotite basal surfaces exposed edge sites, further enhancing basal surface alteration (Figure 2D). More pronounced formations of cracks increased the surface roughness ($R_q$) from ~1.5 to 16.6 nm (Figure 2). For all cases, secondary mineral formations were not significant, except for a very limited quantity of precipitates characterized as amorphous silica and fibrous illite, as reported in our previous study.(14) Thus, the effects of secondary precipitation on roughness changes could be ignored in this study.

Figure 2. AFM images of biotite basal planes after reaction for 70 h in DI water (A), 0.1 M NaCl (B), 0.5 M NaCl (C), and 1.0 M NaCl (D) solutions at 102 atm of $CO_2$and 95 °C. The height scale is 60 nm. $R_q$ is the root-mean-square roughness of the corresponding samples. Static CAs measured at 102 atm of $CO_2$ and 48 °C in 0.1 M NaCl brine for the prereacted biotite flakes as in the top AFM images. Each data point represents the average value of 10 repeated measurements of the $CO_2$ droplet on biotite basal surfaces. The error bar stands for the standard deviation of the measurements.

In addition to morphology changes, dissolution also changed biotite's surface charge. ζ potential measurements (Table S3) show a higher negative charge on biotite powder after reaction at higher salinities, with −19.1 mV for samples reacted in DI water and −47.6 mV for samples reacted in the 1.0 M NaCl solution. As reported by Bray et al., the release of interlayer K is not charge-conservative.(34) More significant ion-exchange reactions occurred at higher salinities, and a larger amount of interlayer K leached into solutions (Figure 1B), resulting in a relative negative charge in the biotite near surface after reactions.

**Chemical Reactions Make Biotite Surfaces More Hydrophilic**

To understand how chemical reactions affect biotite's wettability, we measured high-temperature and high-pressure CAs for the prereacted biotite flakes. The static CAs of biotite basal surfaces decreased with increasing salinity (Figure 2). Previous studies indicated the presence of thin water films on mineral surfaces when $scCO_2$ is injected into deep subsurface reservoirs.(2, 6, 28, 35-37)If a mineral surface can sustain thicker water films, it becomes more hydrophilic. To explain the static CA changes and their relationship to water film thickness, three possible mechanisms can be considered.

First, a reaction-induced roughness increase can decrease the CAs. Surface roughness is a crucial factor impacting surface wettability.(12, 38-41) As indicated by the Wenzel relation, a hydrophilic solid becomes more hydrophilic when the surface roughness is increased.(42)Rougher surfaces can support and stabilize thicker water films through both adsorption and capillarity.(43-45) Compared with those of smooth surfaces, the capillary features of rough surfaces retain the wetting phase better because they can contain more mass in deeper channels. As shown in Figure 2 in our experiments, the biotite surface roughness increased from 1.5 ± 0.2 to 16.6 ± 1.3 nm after high-temperature and high-pressure reactions in DI water and 1.0 M NaCl solutions, respectively. Biotite is a hydrophilic mineral,(46) and a rougher biotite surface can, thus, form thicker water films, with consequently decreased CAs and enhanced wettability.

Second, reaction-induced changes in surface charge can result in CA change. The surface charge can affect water film stability and thickness, with higher-magnitude values supporting thicker films and being important in surface and interface phenomena such as wetting and adhesion. (20)Tokunaga estimated the thickness of water films by considering van der Waals and electric double-layer interactions and found that a decreased surface charge of silica can result in a thinner electric double layer and in substantially thinner adsorbed water films.(20) Similarly, we postulate that the more negatively charged biotite surface due to a significant loss of K after reaction at higher salinity (e.g., −19.1 mV in DI water and −47.6 mV in 1.0 M NaCl) can support thicker water films, making the surface more hydrophilic. Hence, smaller CAs were observed for biotite basal surfaces after reaction at increasing salinities. A caveat was raised concerning the use of the ζ potential measurements of biotite powders in assessing the effect of surface charge on basal surface wettability. Powders have more reactive edge surfaces, and the ζ potential measured is more likely to be from edge surfaces. However, although the extents of the basal and edge surface charge changes might be different, the general trend is expected to be the same for the following reasons: (1) Basal surfaces and edge surfaces were reacted at the same time. (2) The formation of cracks (Figure 2) exposed edges on biotite basal surfaces that could also contribute to the changes in basal surface charges.

Third, surface functional groups interact with the aqueous phase and affect its adsorption to mineral surfaces. Both bridging oxygens (T–O–T; T denotes a tetrahedral site) and terminal oxygens (T–OH) are present on the surface of aluminosilicates.(47, 48) The hydroxyl groups can undergo donor–acceptor interactions with $H_2O$ and make hydrogen bonds; thus, a higher density of hydroxyl groups makes a surface more hydrophilic.(47, 49) In general, breaking of T–O–T linkages is the key step in the dissolution of framework cations in aluminosilicates, and terminal oxygens form.(48, 50) We

hypothesize that dissolution reactions increase the amount of hydroxyl groups, thus making the biotite surface more hydrophilic. From XPS results (Table S4 of the Supporting Information), we observed an increase in the level of hydroxyl groups from around 82.9% (DI) to 92.9% (1.0 M NaCl) on biotite surfaces that reacted at higher salinities. Stronger interactions were expected between water molecules and the biotite surfaces reacted at a higher salinity, leading to more hydrophilic surfaces. Therefore, changes in surface functional groups can also be a mechanism for the increasing hydrophilicity of biotite surfaces.

In summary, reaction-induced roughness, changes in surface charge, and changes in surface functional groups can affect simultaneously and contribute to the more hydrophilic biotite surfaces. Compared to the inconsistency in contact angle values of mica minerals summarized by Iglauer et al.,(1) we suggest that the large uncertainties could come from the different chemical reaction extents of minerals during measurement.

**Reacted Biotite Surfaces Exhibit a Lower $CO_2$ Adhesion and Contact Angle Hysteresis**

Figure 3 shows representative images captured from dynamic CA measurements indicating $CO_2$advancing (water receding) and $CO_2$ receding (water advancing) processes, and the corresponding contact angle hysteresis (CAH) values. The CAH is generally expressed as the difference between the advancing and receding water CAs. A more detailed explanation can be found in section S7 of the Supporting Information. $CO_2$ adhesion refers to the event when the $CO_2$droplet detached from the needle tip and remained attached to the biotite surface when the droplet was retracted by the pump. $CO_2$ adhesion was observed for all biotite samples. However, $CO_2$nonadhesion was also observed on biotite samples that reacted with 1.0 M NaCl solution. $CO_2$adhesion indicates the atomic attractive forces between the contacted surfaces of the sc$CO_2$droplet and the biotite basal surface.(51) The effect of surface roughness on adhesion has been studied, and a decrease in adhesion force with increasing surface roughness was reported. (51-54)Thus, the adhesion force was expected to be lower between sc$CO_2$ and biotite surfaces with a higher roughness after reaction with 1.0 M NaCl, reducing the incidence of $CO_2$ adhesion.

Figure 3. Dynamic CA measurements of biotite samples after reaction for 70 h with different salinities (0, 0.1, 0.5, and 1.0 M NaCl) at 102 atm of $CO_2$ and 95 °C. The CAs were measured in brine with 0.1 M NaCl, at 102

atm of $CO_2$ and 48 °C. (A) These images show $CO_2$ advancing (brine receding), $CO_2$ receding (brine advancing), and $CO_2$ adhesion or nonadhesion on biotite basal surfaces. (B) This table summarizes the dynamic CA measurement results.

The CAH also plays an important role in residual $CO_2$ trapping, including drainage and imbibition processes.(2, 55) During the drainage process, the brine is being displaced, and thus, the water receding CA is representative of this process. Conversely, during the imbibition process, the water advancing CA is operative.(2) Figure 3 shows larger CAH for those biotite samples for which $CO_2$adhesion was observed. The contact line is the ternary phase line among biotite, $CO_2$, and brine. The length of the contact line at the last moment of the $CO_2$ receding process, and before $CO_2$detached from the needle, is shown in Figure 3B. For $CO_2$ adhesion samples, the contact line was pinned (or stuck) to the biotite surface and did not move smoothly. The $CO_2$ droplet detached abruptly from the tip of the needle, leading to longer contact lines. After detachment, the $CO_2$droplet adhered to the biotite surface. Hong et al. suggested that in the captive drop method, the contact line pinning results from CAH (section S7 of the Supporting Information).(56) This suggestion can also explain our finding that $CO_2$ adhesion contributed to larger CAH and to longer contact line on mineral surfaces.(57)

## Environmental Implications

Salinities promote biotite dissolution by enhancing ion-exchange reactions, resulting in larger surface roughness, more negative surface charges, and higher densities of surface hydroxyl groups, which subsequently impact biotite wettability under GCS relevant conditions. This information has important implications for capillary trapping and stratigraphic trapping of $CO_2$ in GCS sites. In subsurface sites, the pores are occupied by brine. After $scCO_2$ is injected, it can enter the pore throats, displacing brine (drainage). When the injection pumps stop, the brine re-enters the pores (imbibition), leaving some $CO_2$ trapped in the pore spaces by capillary forces that is determined by wettability.(2, 58) Moreover, $scCO_2$ may dissolve in brine. The acidified brine can flow into the pores and react with the minerals. Once chemical reactions between $scCO_2$ or acidified brine and minerals cause wettability changes of pores, the increased hydrophilicity leads to higher capillary pressure. In other words, it becomes more difficult for $CO_2$ to diffuse and be transported through porous formations, which is beneficial for the residual trapping of $CO_2$ and sealing of the caprocks. However, there are other factors influencing capillary pressure, such as pore size. Mineral dissolution can

increase the pore size, decreasing the capillary pressure. On the other hand, precipitation can decrease pore size, resulting in the opposite effect.(59)Therefore, property changes of minerals induced by reactions are complicated and should be considered carefully.

During the imbibition process, adhesion of $CO_2$ droplets onto mineral surfaces can immobilize $CO_2$ and increase the level of $CO_2$ residual trapping. Larger CAH leading to more significant $CO_2$contact line pinning will also inhibit $CO_2$ movement. Moreover, in $CO_2$-enhanced oil or gas recovery, $CO_2$ flooding is used to drive oil movement and promote oil production. On the one hand, inhibition of $CO_2$ movement may decrease the oil displacement efficiency. On the other hand, it may also prevent the bypass flow of $scCO_2$ and thus increase oil recovery. Furthermore, CAH affects the saturation hysteresis during residual $CO_2$ trapping, and this information can aid numerical models that include hysteresis in predicting the $CO_2$ distribution because drainage and imbibition cycles occur during GCS.(60, 61) There is, however, a caveat that adhesion occurring in laboratory scale experiments can be different from the translation of a meniscus during displacement processes in the pore space of rocks. Future systematic scale-up studies should improve our understanding of $CO_2$ adhesion.

Although other mica group minerals differ in elemental composition from biotite and can be less reactive, they share similar subunit structures, containing interlayer, tetrahedral, and octahedral sheets and having perfect cleavage along the {001} basal planes. If these mica group minerals undergo reactions under GCS conditions, the effect of these reactions on wettability can therefore be similar. Thus, a better understanding of the effects of salinity on biotite can help predict the general dissolution trend of other abundant mica group minerals in shales. Additionally, chemical reaction-induced surface changes significantly affect wettability. On the basis of the results of this study, we can also infer that if the chemical reactions triggered smoother surfaces that had fewer surface charges or contained fewer surface hydroxyl groups, there could be a decrease in the hydrophilicity of minerals. Here, for the first time, we experimentally related salinity-induced chemical reactions to the wettability changes of minerals under GCS conditions. Our findings elucidate the relationships among salinity, chemical reactions, and wettability changes of minerals under conditions relevant to energy-related subsurface operations, thus benefiting GCS and oil and gas recovery.

## Supporting Information

The Supporting Information is available free of charge on the ACS Publications website at DOI: 10.1021/acs.estlett.5b00359.

- Details on experimental procedures (PDF)

- **PDF**
  - ez5b00359_si_001.pdf (244.21 kB)

**Effects of Salinity-Induced Chemical Reactions on Biotite Wettability Changes under Geologic $CO_2$ Sequestration Conditions**

figshare

ShareDownload

The authors declare no competing financial interest.

## Acknowledgment

We are grateful for the support from the Center for Nanoscale Control of Geologic $CO_2$, an Energy Frontier Research Center funded by the U.S. Department of Energy, Office of Science, Office of Basic Energy Sciences, via Grant DE-AC02-05CH11231. The authors acknowledge Washington University's Institute of Materials Science & Engineering for use of XPS.

- Reference QuickView

## References

This article references 61 other publications.

1. 1.

   Iglauer, S.; Pentland, C.; Busch, A. $CO_2$ wettability of seal and reservoir rocks and the implications for carbon geo-sequestration *Water Resour. Res.* **2015**, 51, 729– 774 DOI: 10.1002/2014WR015553

   [Crossref], [CAS]

2. 2.

   Tokunaga, T. K.; Wan, J. Capillary pressure and mineral wettability influences on reservoir $CO_2$ capacity *Rev. Mineral. Geochem.* **2013**, 77, 481– 503 DOI: 10.2138/rmg.2013.77.14

[Crossref], [CAS]

3. 3.

Chiquet, P.; Broseta, D.; Thibeau, S. Wettability alteration of caprock minerals by carbon dioxide *Geofluids***2007**, 7, 112– 122 DOI: 10.1111/j.1468-8123.2007.00168.x

[Crossref], [CAS]

4. 4.

Saraji, S.; Goual, L.; Piri, M.; Plancher, H. Wettability of supercritical carbon dioxide/water/quartz systems: simultaneous measurement of contact angle and interfacial tension at reservoir conditions *Langmuir* **2013**,29, 6856– 6866 DOI: 10.1021/la3050863

[ACS Full Text], [CAS]

5. 5.

Bikkina, P. K. Contact angle measurements of $CO_2$–water–quartz/calcite systems in the perspective of carbon sequestration *Int. J. Greenhouse Gas Control* **2011**, 5, 1259– 1271 DOI: 10.1016/j.ijggc.2011.07.001

[Crossref], [CAS]

6. 6.

Tenney, C. M.; Cygan, R. T. Molecular simulation of carbon dioxide, brine, and clay mineral interactions and determination of contact angles *Environ. Sci. Technol.* **2014**, 48, 2035– 2042 DOI: 10.1021/es404075k

[ACS Full Text], [CAS]

7. 7.

McCaughan, J.; Iglauer, S.; Bresme, F. Molecular dynamics simulation of water/$CO_2$-quartz interfacial properties: Application to subsurface gas injection *Energy Procedia* **2013**, 37, 5387– 5402 DOI: 10.1016/j.egypro.2013.06.457

[Crossref], [CAS]

8. 8.

Jung, J.-W.; Wan, J. Supercritical $CO_2$ and ionic strength effects on wettability of silica surfaces: Equilibrium contact angle measurements *Energy Fuels* **2012**, 26, 6053– 6059 DOI: 10.1021/ef300913t

[ACS Full Text], [CAS]

9. 9.

Wang, S.; Edwards, I. M.; Clarens, A. F. Wettability phenomena at the $CO_2$–brine–mineral interface: implications for geologic carbon sequestration *Environ. Sci. Technol.* **2013**, 47, 234– 241 DOI: 10.1021/es301297z

[ACS Full Text], [CAS]

10. 10.

Espinoza, D. N.; Santamarina, J. C. Water-$CO_2$-mineral systems: Interfacial tension, contact angle, and diffusion—Implications to $CO_2$ geological storage *Water Resour. Res.* **2010**, 46, 1– 10 DOI: 10.1029/2009WR008634

[Crossref]

11. 11.

Wan, J.; Kim, Y.; Tokunaga, T. K. Contact angle measurement ambiguity in supercritical $CO_2$–water–mineral systems: Mica as an example *Int. J. Greenhouse Gas Control* **2014**, 31, 128– 137 DOI: 10.1016/j.ijggc.2014.09.029

[Crossref], [CAS]

12. 12.

Spori, D. M.; Drobek, T.; Zürcher, S.; Ochsner, M.; Sprecher, C.; Mühlebach, A.; Spencer, N. D. Beyond the lotus effect: roughness influences on wetting over a wide surface-energy range *Langmuir* **2008**, 24, 5411–5417 DOI: 10.1021/la800215r

[ACS Full Text], [CAS]

13. 13.

Iglauer, S.; Salamah, A.; Sarmadivaleh, M.; Liu, K.; Phan, C. Contamination of silica surfaces: Impact on water–$CO_2$–quartz and glass contact angle measurements *Int. J. Greenhouse Gas Control* **2014**, 22, 325–328 DOI: 10.1016/j.ijggc.2014.01.006

[Crossref], [CAS]

14. 14.

Hu, Y.; Ray, J. R.; Jun, Y. S. Biotite-brine interactions under acidic hydrothermal conditions: fibrous Illite, goethite, and kaolinite formation and biotite surface cracking *Environ. Sci. Technol.* **2011**, 45, 6175– 80 DOI: 10.1021/es200489y

[ACS Full Text], [CAS]

15. 15.

Hu, Y.; Ray, J. R.; Jun, Y. S. $Na^+$, $Ca^{2+}$, and $Mg^{2+}$ in brines affect supercritical $CO_2$-brine-biotite interactions: ion exchange, biotite dissolution, and Illite precipitation *Environ. Sci. Technol.* **2013**, 47, 191– 7 DOI: 10.1021/es301273g

[ACS Full Text], [CAS]

16. 16.

Shiraki, R.; Dunn, T. L. Experimental study on water–rock interactions during $CO_2$ flooding in the Tensleep Formation, Wyoming, USA *Appl. Geochem.* **2000**, 15, 265– 279 DOI: 10.1016/S0883-2927(99)00048-7

[Crossref], [CAS]

17. 17.

Yang, Y.; Ronzio, C.; Jun, Y.-S. The effects of initial acetate concentration on $CO_2$–brine–anorthite interactions under geologic $CO_2$ sequestration conditions *Energy Environ. Sci.* **2011**, 4, 4596– 4606 DOI: 10.1039/c1ee01890f

[Crossref], [CAS]

18. 18.

Yang, Y.; Min, Y.; Jun, Y.-S. Structure-dependent interactions between alkali feldspars and organic compounds: implications for reactions in geologic carbon sequestration *Environ. Sci. Technol.* **2013**, 47,150– 158 DOI: 10.1021/es302324m

[ACS Full Text], [CAS]

19. 19.

Min, Y.; Kubicki, J. D.; Jun, Y.-S. Plagioclase Dissolution during $CO_2$-$SO_2$ Co-sequestration: Effects of Sulfate *Environ. Sci. Technol.* **2015**, 49, 1946– 1954 DOI: 10.1021/es504586u

[ACS Full Text], [CAS]

20. 20.

Tokunaga, T. K. DLVO-based estimates of adsorbed water film thicknesses in geologic $CO_2$ reservoirs*Langmuir* **2012**, 28, 8001– 8009 DOI: 10.1021/la2044587

[ACS Full Text], [CAS]

21. 21.

Bachu, S.; Adams, J. Sequestration of $CO_2$ in geological media in response to climate change: capacity of deep saline aquifers to sequester $CO_2$ in solution *Energy Convers. Manage.* **2003**, 44, 3151– 3175 DOI: 10.1016/S0196-8904(03)00101-8

[Crossref], [CAS]

22. 22.

White, C. M.; Strazisar, B. R.; Granite, E. J.; Hoffman, J. S.; Pennline, H. W. Separation and capture of $CO_2$from large stationary sources and sequestration in geological formations—

coalbeds and deep saline aquifers *J. Air Waste Manage. Assoc.* **2003**, 53, 645– 715 DOI: 10.1080/10473289.2003.10466206

[Crossref], [PubMed], [CAS]

23. 23.

Metz, B.; Davidson, O.; De Coninck, H.; Loos, M.; Meyer, L. IPCC special report on carbon dioxide capture and storage: Prepared by Working Group III of the Intergovernmental Panel on Climate Change; IPCC:Cambridge, U.K., **2005**.

24. 24.

Benson, S. M.; Cole, D. R. $CO_2$ sequestration in deep sedimentary formations *Elements* **2008**, 4, 325– 331DOI: 10.2113/gselements.4.5.325

[Crossref], [CAS]

25. 25.

Emberley, S.; Hutcheon, I.; Shevalier, M.; Durocher, K.; Mayer, B.; Gunter, W.; Perkins, E. Monitoring of fluid–rock interaction and $CO_2$ storage through produced fluid sampling at the Weyburn $CO_2$-injection enhanced oil recovery site, Saskatchewan, Canada *Appl. Geochem.* **2005**, 20, 1131– 1157 DOI: 10.1016/j.apgeochem.2005.02.007

[Crossref], [CAS]

26. 26.

Harrison, W. J.; Summa, L. L. Paleohydrology of the Gulf of Mexico basin *Am. J. Sci.* **1991**, 291, 109– 176DOI: 10.2475/ajs.291.2.109

[Crossref]

27. 27.

Kharaka, Y. K.; Thordsen, J. J.; Hovorka, S. D.; Seay Nance, H.; Cole, D. R.; Phelps, T. J.; Knauss, K. G.Potential environmental issues of $CO_2$ storage in deep saline aquifers: Geochemical results from the Frio-I Brine Pilot test, Texas, USA *Appl. Geochem.* **2009**, 24, 1106– 1112 DOI: 10.1016/j.apgeochem.2009.02.010

[Crossref], [CAS]

28. 28.

Shao, H.; Ray, J. R.; Jun, Y.-S. Effects of salinity and the extent of water on supercritical $CO_2$-induced phlogopite dissolution and secondary mineral formation *Environ. Sci. Technol.* **2011**, 45, 1737– 1743 DOI: 10.1021/es1034975

[ACS Full Text], [CAS]

29. 29.

Icenhower, J. P.; Dove, P. M. The dissolution kinetics of amorphous silica into sodium chloride solutions: effects of temperature and ionic strength *Geochim. Cosmochim. Acta* **2000**, 64, 4193– 4203 DOI: 10.1016/S0016-7037(00)00487-7

[Crossref], [CAS]

30. 30.

Espinoza, D. N.; Santamarina, J. C. Water–$CO_2$–mineral systems: Interfacial tension, contact angle, and diffusion—Implications to $CO_2$ geological storage *Water Resour. Res.* **2010**, 46, W07537 DOI: 10.1029/2009WR008634

[Crossref], [CAS]

31. 31.

Hu, Y.; Jun, Y. S. Biotite dissolution in brine at varied temperatures and $CO_2$ pressures: its activation energy and potential $CO_2$ intercalation *Langmuir* **2012**, 28, 14633– 41 DOI: 10.1021/la3028995

[ACS Full Text], [CAS]

32. 32.

Zhang, L.; Jun, Y.-S. Distinctive Reactivities at Biotite Edge and Basal Planes in the Presence of Organic Ligands: Implications for Organic-Rich Geologic $CO_2$ Sequestration *Environ. Sci. Technol.* **2015**, 49, 10217–10225 DOI: 10.1021/acs.est.5b01960

[ACS Full Text], [CAS]

33. 33.

Bradshaw, J.; Cook, P. Geological sequestration of carbon dioxide *Environ. Geosci.* **2001**, 8, 149– 151 DOI: 10.1046/j.1526-0984.2001.008003149.x

[Crossref]

34. 34.

Bray, A. W.; Benning, L. G.; Bonneville, S.; Oelkers, E. H. Biotite surface chemistry as a function of aqueous fluid composition *Geochim. Cosmochim. Acta* **2014**, 128, 58– 70 DOI: 10.1016/j.gca.2013.12.002

[Crossref], [CAS]

35. 35.

Loring, J. S.; Thompson, C. J.; Wang, Z.; Joly, A. G.; Sklarew, D. S.; Schaef, H. T.; Ilton, E. S.; Rosso, K. M.;Felmy, A. R. In situ infrared spectroscopic study of forsterite carbonation in wet supercritical $CO_2$ *Environ. Sci. Technol.* **2011**, 45, 6204– 6210 DOI: 10.1021/es201284e

[ACS Full Text], [CAS]

36. 36.

Hamm, L. M.; Bourg, I. C.; Wallace, A. F.; Rotenberg, B. Molecular simulation of $CO_2^-$ and $CO_3^-$ brine-mineral systems *Rev. Mineral. Geochem.* **2013**, 77, 189– 228 DOI: 10.2138/rmg.2013.77.6

[Crossref], [CAS]

37. 37.

Kim, T. W.; Tokunaga, T. K.; Shuman, D. B.; Sutton, S. R.; Newville, M.; Lanzirotti, A. Thickness measurements of nanoscale brine films on silica surfaces under geologic $CO_2$ sequestration conditions using synchrotron X-ray fluorescence *Water Resour. Res.* **2012**, 48, 48 DOI: 10.1029/2012WR012200

[Crossref]

38. 38.

Hitchcock, S.; Carroll, N.; Nicholas, M. Some effects of substrate roughness on wettability *J. Mater. Sci.***1981**, 16, 714– 732 DOI: 10.1007/BF02402789

[Crossref], [CAS]

39. 39.

Nakae, H.; Inui, R.; Hirata, Y.; Saito, H. Effects of surface roughness on wettability *Acta Mater.* **1998**, 46,2313– 2318 DOI: 10.1016/S1359-6454(97)00387-X

[Crossref], [CAS]

40. 40.

Quéré, D. Wetting and roughness *Annu. Rev. Mater. Res.* **2008**, 38, 71– 99 DOI: 10.1146/annurev.matsci.38.060407.132434

[Crossref], [CAS]

41. 41.

Quéré, D. Rough ideas on wetting *Phys. A* **2002**, 313, 32– 46 DOI: 10.1016/S0378-4371(02)01033-6

[Crossref], [CAS]

42. 42.

Wenzel, R. N. Resistance of solid surfaces to wetting by water *Ind. Eng. Chem.* **1936**, 28, 988– 994 DOI: 10.1021/ie50320a024

[ACS Full Text], [CAS]

43. 43.

Garoff, S.; Sirota, E.; Sinha, S.; Stanley, H. The effects of substrate roughness on ultrathin water films *J. Chem. Phys.* **1989**, 90, 7505– 7515 DOI: 10.1063/1.456184

[Crossref], [CAS]

44. 44.

Philip, J. Adsorption and capillary condensation on rough surfaces *J. Phys. Chem.* **1978**, 82, 1379– 1385DOI: 10.1021/j100501a012

[ACS Full Text], [CAS]

45. 45.

Kim, T. W.; Tokunaga, T. K.; Bargar, J. R.; Latimer, M. J.; Webb, S. M. Brine film thicknesses on mica surfaces under geologic $CO_2$ sequestration conditions and controlled capillary pressures *Water Resour. Res.* **2013**, 49, 5071– 5076 DOI: 10.1002/wrcr.20404

[Crossref], [CAS]

46. 46.

Mills, J.; Riazi, M.; Sohrabi, M. Wettability of common rock-forming minerals in a $CO_2$-brine system at reservoir conditions *Soc. Core Analysts* **2011**, 1– 12

47. 47.

Zhuravlev, L. The surface chemistry of amorphous silica. Zhuravlev model *Colloids Surf., A* **2000**, 173, 1–38 DOI: 10.1016/S0927-7757(00)00556-2

[Crossref], [CAS]

48. 48.

Xiao, Y.; Lasaga, A. C. Ab initio quantum mechanical studies of the kinetics and mechanisms of silicate dissolution: $H^+(H_3O^+)$ catalysis *Geochim. Cosmochim. Acta* **1994**, 58, 5379– 5400 DOI: 10.1016/0016-7037(94)90237-2

[Crossref], [CAS]

49. 49.

Chen, C.; Zhang, N.; Li, W.; Song, Y. Water Contact Angle Dependence with Hydroxyl Functional Groups on Silica Surfaces under $CO_2$ Sequestration Conditions *Environ. Sci. Technol.* **2015**, 49, 14680– 14687 DOI: 10.1021/acs.est.5b03646

[ACS Full Text], [CAS]

50. 50.

Brantley, S. L.; Kubicki, J. D.; White, A. F. *Kinetics of water-rock interaction*; Springer: Menlo Park, CA,**2008**.

[Crossref]

51. 51.

Kendall, K. Adhesion: molecules and mechanics *Science* **1994**, 263, 1720– 1725 DOI: 10.1126/science.263.5154.1720

[Crossref], [PubMed], [CAS]

52. 52.

Roy Chowdhury, S. K.; Pollock, H. Adhesion between metal surfaces: the effect of surface roughness *Wear***1981**, 66, 307– 321 DOI: 10.1016/0043-1648(81)90124-1

[Crossref]

53. 53.

Rabinovich, Y. I.; Adler, J. J.; Ata, A.; Singh, R. K.; Moudgil, B. M. Adhesion between nanoscale rough surfaces: II. Measurement and comparison with theory *J. Colloid Interface Sci.* **2000**, 232, 17– 24 DOI: 10.1006/jcis.2000.7168

[Crossref], [PubMed], [CAS]

54. 54.

Wang, S.; Tao, Z.; Persily, S. M.; Clarens, A. F. $CO_2$ adhesion on hydrated mineral surfaces *Environ. Sci. Technol.* **2013**, 47, 11858– 11865 DOI: 10.1021/es402199e

[ACS Full Text], [CAS]

55. 55.

Gao, L.; McCarthy, T. J. Contact angle hysteresis explained *Langmuir* **2006**, 22, 6234– 6237 DOI: 10.1021/la060254j

[ACS Full Text], [CAS]

56. 56.

Hong, S.-J.; Chang, F.-M.; Chou, T.-H.; Chan, S. H.; Sheng, Y.-J.; Tsao, H.-K. Anomalous contact angle hysteresis of a captive bubble: advancing contact line pinning *Langmuir* **2011**, 27, 6890– 6896 DOI: 10.1021/la2009418

[ACS Full Text], [CAS]

57. 57.

Broseta, D.; Tonnet, N.; Shah, V. Are rocks still water-wet in the presence of dense $CO_2$ or $H_2S$? *Geofluids***2012**, 12, 280– 294 DOI: 10.1111/j.1468-8123.2012.00369.x

[Crossref], [CAS]

58. 58.

Jun, Y.-S.; Giammar, D. E.; Werth, C. J. Impacts of geochemical reactions on geologic carbon sequestration*Environ. Sci. Technol.* **2013**, 47, 3– 8 DOI: 10.1021/es3027133

[ACS Full Text ], [CAS]

59. 59.

Shao, H.; Jun, Y. S. Mineral dissolution and nanoparticle evolution on phlogopite surfaces under $CO_2$geologic sequestration conditions *Geochim. Cosmochim. Acta* **2010**, 74, A940– A940

60. 60.

Doughty, C. Modeling geologic storage of carbon dioxide: comparison of non-hysteretic and hysteretic characteristic curves *Energy Convers. Manage.* **2007**, 48, 1768– 1781 DOI: 10.1016/j.enconman.2007.01.022

[Crossref], [CAS]

61. 61.

Ruprecht, C.; Pini, R.; Falta, R.; Benson, S.; Murdoch, L. Hysteretic trapping and relative permeability of $CO_2$ in sandstone at reservoir conditions *Int. J. Greenhouse Gas Control* **2014**, 27, 15– 27 DOI: 10.1016/j.ijggc.2014.05.003

[Crossref], [CAS]